(This is a sample cover image for this issue. The actual cover is not yet available at this time.)

Spectrochimica Acta Part A: Molecular and Biomolecular Spectroscopy 97 (2012) 1089–1100

Contents lists available at SciVerse ScienceDirect

Spectrochimica Acta Part A: Molecular and Biomolecular Spectroscopy

journal homepage: www.elsevier.com/locate/saa

Interaction between holo transferrin and HSA–PPIX complex in the presence of lomefloxacin: An evaluation of PPIX aggregation in protein–protein interactions

Zohreh Sattar [a], Hediye Iranfar [a], Ahmad Asoodeh [b], Mohammad Reza Saberi [c], Mahboobeh Mazhari [d], Jamshidkhan Chamani [a,*]

[a] Department of Biology, Faculty of Sciences, Mashhad Branch, Islamic Azad University, Mashhad, Iran
[b] Department of Chemistry, Faculty of Sciences, Ferdowsi University of Mashhad, Mashhad, Iran
[c] Medical Chemistry Department, School of Pharmacy, Mashhad University of Medical Sciences, Mashhad, Iran
[d] Faculty of Agriculture and Natural Resources, Karaj Branch, Islamic Azad University, Karaj, Iran

HIGHLIGHTS

- We studied the interaction between HSA and TF, in the presence of PPIX and LMF.
- Our results showed that the PPIs increased at low concentration of LMF.
- The binding affinity of LMF to HSA–PPIX was lower than to HSA.
- The RLS technique was utilized to investigate the effect of LMF on aggregation of PPIX.
- The conformational change of protein upon binding was monitored as a function of added drug.

GRAPHICAL ABSTRACT

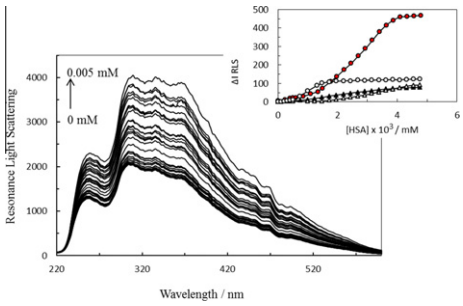

ARTICLE INFO

Article history:
Received 26 April 2012
Received in revised form 8 July 2012
Accepted 10 July 2012
Available online 4 August 2012

Keywords:
HSA
Holo transferrin
Fluorescence quenching
Zeta-potential
Protein–protein interaction

ABSTRACT

Human serum albumin (HSA) and holo transferrin (TF) are two serum carrier proteins that are able to interact with each other, thereby altering their binding behavior toward their ligands. During the course of this study, the interaction between HSA–PPIX and TF, in the presence and absence of lomefloxacin (LMF), was for the first time investigated using different spectroscopic and molecular modeling techniques. Fluorescence spectroscopy experiments were performed in order to study conformational changes of proteins. The RLS technique was utilized to investigate the effect of LMF on J-aggregation of PPIX, which is the first report of its kind. Our findings present clear-cut evidence for the alteration of interactions between HSA and TF in the presence of PPIX and changes in drug-binding to HSA and HSA–PPIX complex upon interaction with TF. Moreover, molecular modeling studies suggested that the binding site for LMF became switched in the presence of PPIX, and that LMF bound to the site IIA of HSA. The obtained results should give new insight into research in this field and may cast some light on the dynamics of drugs in biological systems.

Abbreviations: HSA, human serum albumin; TF, holo transferrin; PPIX, protoporphyrin X; PPIs, protein protein interactions; LMF, lomefloxacin.

* Corresponding author. Tel.: +98 511 8437107; fax: +98 511 8424020.
E-mail addresses: chamani@ibb.ut.ac.ir, chamani_J@yahoo.com (J. Chamani).

1386-1425/$ - see front matter © 2012 Elsevier B.V. All rights reserved.
http://dx.doi.org/10.1016/j.saa.2012.07.034

Introduction

Protein–protein interactions (PPIs) are one of the most important phenomena sustaining many biological processes such as the assembly of cellular components, the transport machinery across the various biological membranes, signal transduction and the regulation of gene expression and enzymatic activities [1]. On the other hand, the binding of drugs to serum proteins is particularly important since it affects both the activity of the drugs and their disposition [2]. Serum proteins play a dominant role in transport and disposition of various dyes and drugs in blood. Human serum albumin (HSA) and transferrin (TF) are the most abundant proteins in blood plasma and are able to bind and transport various ligands, especially drugs [3]. Moreover, there is evidence of conformational changes of serum protein induced by its interaction with ligands and/or other proteins in plasma, which appears to affect the secondary and tertiary structure of these proteins [4].

Lomefloxacin (LMF) (Fig. 1) (with the molecular formula $C_{17}H_{19}F_2N_3O_3$; molecular weight of 351.348 g/mol) is a third-generation member of quinolone antibiotics fluorinated in position 6 and bearing a piperazinyl moiety in position 7, capable of penetrating well into cells [5]. LMF is very active against both Gram (+) and Gram (−) bacteria through inhibition of their DNA gyrase and is widely used for the clinical treatment of severe systematic infections, such as soft tissue infection, typhoid fever, bone and joint infections, prostatitis blood poisoning and sinusitis [5].

Transferrin (TF) is one of the monomeric serum proteins, containing 679 amino acid residues, with a serum concentration of 2.5 mg ml^{-1}. This protein is mainly responsible for transport of metal ions and minerals [6–8]. It is divided into two lobes (N- and C-lobes), each of which contains two domains comprising a series of α-helices and β-sheets. TF has 8 Trp residues and is stabilized by 19 intra-chain disulfide bonds [9].

HSA (with a molecular weight 66,479 Da) [10] is a principal extracellular protein with a high concentration in blood plasma (40 mg ml^{-1} or 0.6 mM) [11]. It is a single-string globular protein possessing 585 amino acids, in which 35 cysteines constitute 17 disulfide bridges, and assume solid equilateral triangular shapes with sides ≈80 Å and depths ≈30 Å [12]. The three-dimensional structure of HSA can be considered as an ensemble of three globular domains, namely IA, IB; IIA, IIB; IIIA and IIIB, freely linked by extended random coils. There is only one Trp located at position 214, in subdomain IIA of HSA [13]. This structural organization provides a variety of ligand binding sites. Bulky heterocyclic anions bind preferentially to site I, whereas site II is preferred by aromatic carboxylates with an extended conformation.

Protoporphyrin IX (PPIX) is the iron-free form of heam, one of the most common natural sources of porphyrin [14], and important endogenous ligands transported and/or sequestered by human albumin. PPIX binds strongly to the HSA primary binding site located at the interface between domain I and II, within a narrow D-shaped hydrophobic cavity. They are applied in medicine an important areas as cancer detection and as photosensitizers in photodynamic therapy of cancer biological effects of porphyrins largely depend on their physicochemical properties, which in turn lead to important changes in their photophysical behavior. Porphyrins are usually introduced in the blood as relatively concentrated solutions, which may diminish its action or even cause adverse effects. Moreover, interactions with macromolecules may control the efficacy and biodistribution of porphyrins, which are known to locate preferentially in the cytoplasm and bind poorly to cell membranes. Therefore the interaction of these molecules with proteins, especially those that provide carriage through the blood stream, is almost importance of formulate safe drugs and effective dosages [15–17]. Furthermore, PPIX binds to HSA rendering it possible for HSA–PPIX complex to be produced with HSA in serum. Ligand binding to one domain induces distinct conformational changes in the other domain, as both sub-domains share a common interface. Thus, the binding of a particular drug molecule to serum albumin may considerably change binding abilities of HSA towards other molecules [2,18].

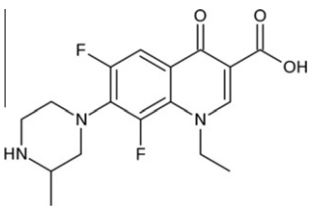

Fig. 1. Structure of lomefloxacin.

It was demonstrated that the HSA and TF could interact with each other and that LMF could induce conformational transitions in both proteins in such a way and could also strengthen the HSA–TF interaction [7,9]. However, in serum, the HSA is also available in the form of HSA–PPIX complex as mentioned above. Therefore, the aim of this study has been to explore whether or not the presence of PPIX could change the interaction found in our previously investigation that play a major role in determining usage dose of LMF.

Our results represent clear-cut evidence regarding the role of PPIX in the interaction between HSA and TF as well as in the interaction of LMF to these two carrier proteins, whether separate or simultaneous together. The important outcome of this work is in its details of the interaction mechanism, which is studied using multi-spectroscopic, zeta potential and molecular modeling.

Experimental section

Chemicals

HSA, TF, protoporphyrin IX (PPIX), lomefloxacin (LMF) and potassium phosphate were purchased from Sigma Chemical Company. (St. Louis, Mo, USA), and used without further purification. Dimethyl formamide (DMF), sodium carbonate, ethylene diamine tetra-acetic acid (EDTA), ethanol and sodium hydroxide were obtained from Merck Chemical Co. (Germany). Visking dialysis tubing was obtained from Scientific Instrument Center Limited (SIC, Eastleigh, UK). Double-distilled water was used throughout the experiments.

Sample preparation

HSA (4.5×10^{-6} M), HSA–PPIX complex (4.5×10^{-3} mM) and TF (4.5×10^{-3} mM), were dissolved in a 50-mM phosphate buffer solution at pH 7.4. Various concentrations of LMF were obtained by diluting a stock solution of LMF (0.5 mM) in 50-mM phosphate buffer. For the drug–protein interaction studies, a 2.0-ml protein solution (the concentration of proteins was maintained at (4.5×10^{-3} mM) was titrated by addition of 10-μl volumes of 0.05-mM LMF. For the PPI studies, a 2.0-ml solution of TF (4.5×10^{-3} mM) with or without LMF (at one of the following concentrations: 0.003, 0.006, 0.009 mM) was titrated by addition of a 100.5×10^{-3} mM stock solution of HSA–PPIX complex and/or HSA. All protein solutions were freshly and samples were measured at room temperature. The extinction coefficients were used to calculate the concentration of the native protein. If the initial concentration and volume of the protein solution are $[P]_0$ and V_0 respectively, and the stock ligand concentration is $[L]_0$, then the total concentration of protein ($[P]_t$) and ligand ($[L]_t$) can be obtained

by accounting for the total volume of the aliquot (V_c) added during the titration experiment [19].

$$[P]_t = [P]_0 V_0/(V_0 + V_c), [L]_t = [L]_0 V_0/(V_0 + V_c)$$

HSA was labeled with PPIX as reported previously [10]: 3.5 mg of PPIX was dissolved in 100-μl DMF and injected in five aliquots of 20 μl each to 2 ml of phosphate buffer containing 200-μM HSA in intervals of 15 min under vigorous stirring. The mixture was stirred for 1 h after which a mild dialysis was carried out against phosphate buffer for 4.5 h to remove the unreacted PPIX [10].

Methods

Fluorescence spectroscopy

Fluorescence measurements were performed with an F-2500 spectrofluorimeter (Hitachi, Japan) with a 150 W Xenon lamp, a 1.0-cm quartz cell and a thermostatic bath. The widths of both the excitation slit and emission slit were set at 5.0 nm. The operation software automatically corrected the spectral scan for the photomultiplier characteristic. Furthermore, fluorescence intensities were corrected for inner filter and dilution effects before any data analysis was carried out. In the fluorescence measurements, the excitation wavelengths were set to 280 and 295 nm and the scan speed was 500 nm/min. The three dimensional fluorescence spectrum were recorded with a FP-6200 spectrofluorometer (Jasco, Japan) equipped with a 150 W Xenon lamp. A 1-cm quarts cuvette with four optical windows was used for the analyses. Emission scans were performed from 220 to 500 nm at 5 nm steps, with excitation wavelengths from 220 to 500 nm in intervals. The detector was set to high sensitivity. The slit widths for excitation and emission were 5 nm, and the experiments were performed under some conditions as the fluorescence spectroscopy.

UV–visible spectrophotometry

Absorbance measurements were carried out with a Jasco spectrophotometer (V630, Japan), equipped with a 1.0-cm quartz cell. The optical system was based on a split-beam with a gating band width of 5 nm. The light source was a Xenon lamp. All measurements were performed at room temperature.

Resonance light scattering (RLS)

The RLS spectra were recorded by simultaneously scanning excitation and emission wavelengths ($\Delta\lambda = 0$). The enhancement RLS intensity (ΔIRLS) is represented as [20]:

$$\Delta I_{RLS} = I_{RLS} - I^0_{RLS} \quad (1)$$

where I_{RLS} and I^0_{RLS} are the RLS intensity of the system in the presence and absence of drugs, respectively. RLS has proven to be an elegant technique in order to investigate the aggregation of small molecules as well as the long-range assembly of drugs on biological templates.

Circular dichroism spectroscopy

Circular dichroism (CD) measurements were carried out on a Jasco J-815 automatic recording spectropolarimeter (Jasco, Japan). Spectra were recorded on protein samples with concentrations of 0.01% in a 1-cm path length quartz cuvette. A band width of 1 nm and a response of 2 s were used, with a scanning rate at 50 nm min^{-1} to obtain final spectra as an average of five scans. To explore changes in the secondary structure, far-UV CD spectra were obtained over a wavelength range of 190–240 nm. The secondary structure contents of protein have been analyzed by SILCON III software method. For the drug–protein studies, a protein solution (HSA, HSA–PPIX complex and TF) was titrated by five aliquots of 0.016-mM LMF. For the PPI studies, a mixture of 2.0 ml of a solution containing TF protein (0.01%) in the presence and absence of LMF at three different concentrations (0.001, 0.002, 0.003 mM) was titrated by addition of aliquots of 33.5×10^{-3}-mM solutions of HSA–PPIX complex. Moreover, in another set of experiments, it was titrated by 33.5×10^{-3}-mM HSA.

Zeta potential analyses

Particle size, polydispersity and zeta potential measurements were conducted using a Malvern Zeta-sizer. The analyses were performed at ambient temperature. The Henry equation was used to calculate zeta-potentials from measurements of the electrophoretic mobility [62]. In this calculation, the viscosity of the solution was assumed to be the same as that of water.

Molecular modeling

The docking calculations of the association of LMF with HSA, HSA–PPIX complex and TF were undertaken using the Autodock4 program. The crystal structures of HSA, HSA–PPIX complex and TF were retrieved from the RCSB Protein Data Bank (PDB entry: 1ao6, 1n5u, 1suv respectively). The protein–protein docking program HEX v.5.1, was subsequently used to examine probable modes of interaction between HSA–PPIX complex and TF in the presence of LMF. To model the effect of LMF on the interaction between HSA–PPIX complex and TF, the complexes of TF–LMF were applied to energy minimization with an MM+ force field. Finally, the best docking results were applied to WebLab-Viewer Lite, Molegro Molecular Viewer and Swiss pdb-Viewer 4 for further investigations. The drug was drawn, and then copied in Chem 3D, which is another production of Cambridge Soft 2007.

Results and discussion

RLS analysis

RLS is a valuable technique for detecting and characterizing self-assemblies and extended aggregates of chromophores since these assemblies or aggregations lead to the formation of large fractal structures exhibiting strong RLS signals [18,20–22]. RLS spectra of titration of TF with HSA (Fig. 2A) and HSA–PPIX complex (Fig. 2B) in the absence and presence of LMF at three concentrations were obtained (303 nm was applied to the determination). As can be seen from Fig. 2A, the addition of HSA enhanced the RLS peaks. Since the amount of scattering is directly proportional to the volume of each sphere [5,17], these observations pointed at the long-range assembly of HSA on the molecular surface of TF and on an enlargement of the molecular volume. The spectra for the TF–HSA system indicated that there were interactions among these substances and that an HSA–TF complex was formed. Moreover, a general decrease in ΔI_{RLS} was observed with the increase in concentration of LMF. It was noted that in the presence of LMF at a low concentration (0.003 mM), with an increase in HSA concentration up to 1.7×10^{-3} mM, there was first an increase in PPI, after which it was constant. In order to decipher the effect of PPIX on the interaction between these two proteins and its inter-relationship with the concentration of LMF, RLS spectra of the TF–(HSA–PPIX) complex system in the absence and presence of LMF were also obtained (Fig. 2B). As can be seen, adding HSA–PPIX complex up to $\sim 2 \times 10^{-3}$ mM led to a regular increase of the RLS signals, which indicated increasing amounts of protein–protein complex formations. However, at higher concentrations, the intensities decreased back to the initially observed signal level.

Moreover, the effect of the different concentrations of LMF on the RLS spectra of the TF–(HSA–PPIX) complex system is shown in Fig. 2B. As was also seen for the HSA–TF system, LMF did not have a definite effect on the (HSA–PPIX)–TF interactions. Probably,

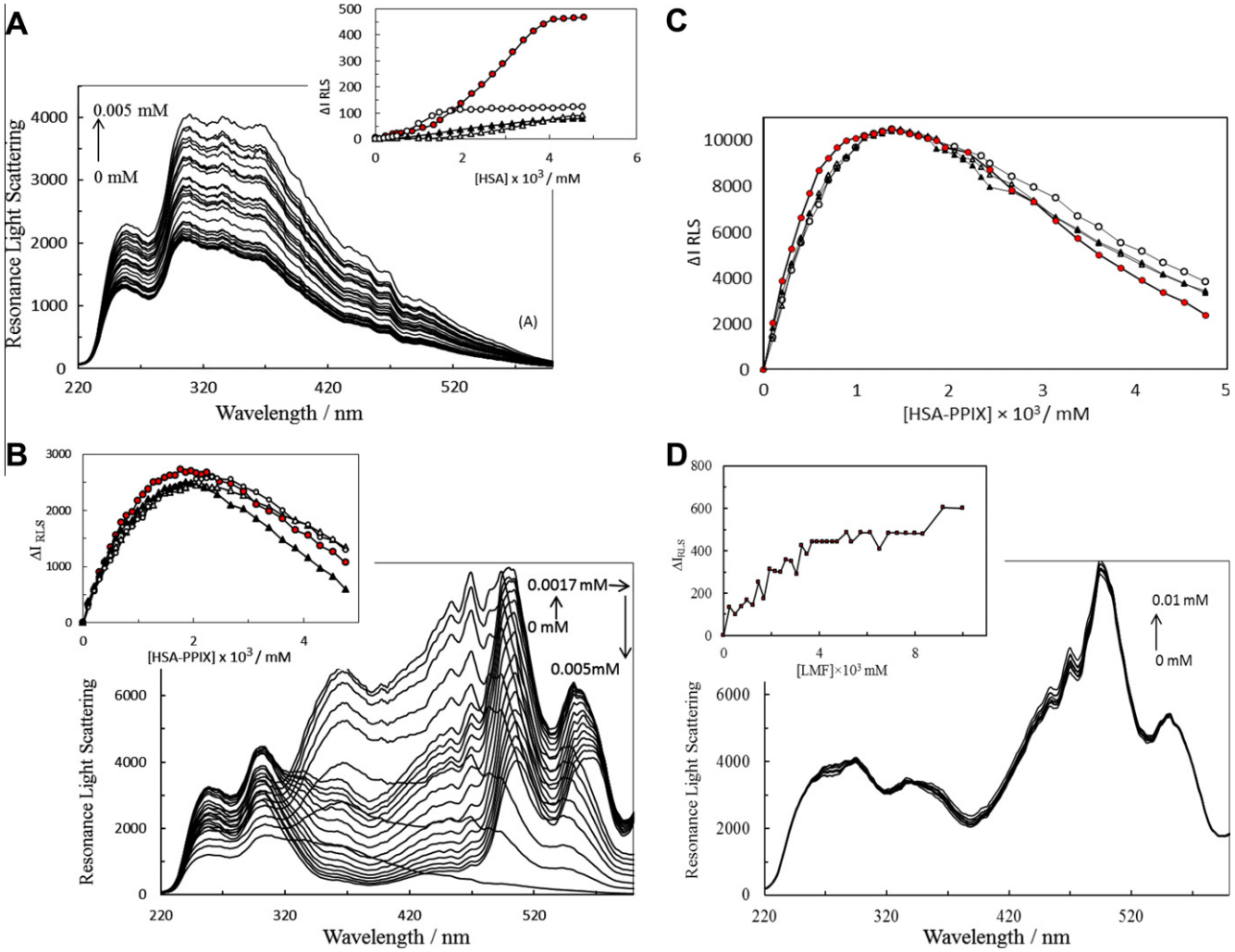

Fig. 2. (A) RLS spectra of the interaction of the HSA with TF. (Inset: effect of LMF on HSA–TF interaction). (B) RLS spectra of the interaction of HSA–PPIX with TF. (Inset: effect of LMF on [(HSA–PPIX)–TF interaction]) (C) J-bond plot of the interaction of HSA–PPIX with TF in the absence and presence of LMF. (D) RLS spectra of the interaction of HSA–PPIX with LMF. (Inset: J-bond plot of the interaction of HSA–PPIX with LMF). TF filled circle, [TF–LMF (0.003 mM)] open circle, [TF–LMF (0.006 mM)] filled triangle, [TF–LMF (0.009 mM)] open triangle. The intensity difference of RLS have been calculated at $\lambda = 303$ nm.

the presence of PPIX interfered with the observation of LMF effects. As can be observed in Fig. 2B, a new peak located at about 490 nm was observed after addition of HSA–PPIX complex. The RLS spectrum at that wavelength point to the existence of a nonaggregated species, which rise from the protonation of both the propionate end groups and the two nitrogen atoms of the core. This finding seems in contrast with the behavior of other water soluble porphyrins, such as the tetrakis (p-carboxyphenyl) porphine (TCPP) [23], and tetrakis (p-sulfonatophenyl) porphine (TPPS) [25], which under strong acidic conditions from extended J-aggregates [24], these results are easily understood since the structure of the protonated macro cycle of porphyrin was more planar than that of the unprotonated structure of porphyrin, namely, a planar structure of an aromatic molecule was more conductive due to the formation of aggregates in aqueous solution [25–29]. J-aggregates formed with the monomeric molecules arranged in one dimension such that the transition moment of the monomers was parallel and the angle between the transition moment and the line joining the molecular centers was zero (ideal case). In contrast to the side-by-side arrangement of molecules in J-aggregates, the arrangement in H-aggregates was face-to-face [25,30,31]. As observed in Fig. 2C, the RLS intensity at that wavelength (490 nm) increased up to a concentration of 1.4×10^{-3} mM of HSA–PPIX complex and remained constant up to 2×10^{-3} mM followed by a decrease with further addition of HSA–PPIX complex. This implied that PPIX J-aggregates were effectively induced in the concentration range of $1–2 \times 10^{-3}$ mM of HSA–PPIX complex. As explained previously (Fig. 2B), an almost identical concentration range was observed for PPI in the presence of the PPIX molecule, and it therefore seemed that the two phenomena of PPI and J-aggregation were coupled. However, further studies are required in order to unravel this coupling mechanism in detail.

To further understand the above results, the effect of LMF on the RLS spectra of HSA–PPIX complex were obtained in a separate experiment and the results are shown in Fig. 2D. As can be inferred from the spectra, with addition of LMF, the intensities at 490 nm wavelength increased regularly (Fig. 2D inset).

LMF has two pK_a values; 5.7 and 7.9 and the existence ratio of their zwitterionic forms are higher under neutral conditions (75% at pH = 7.4) than in acidic environments [32]. We know that most of the LMF bound with high affinity to the IB sub-domain and this is explained in the section on molecular modeling. On the other hand, the structure revealed that the PPIX bound to a single site within a hydrophobic cavity in sub-domain IB [12]. Obviously, the electrostatic interaction played an important role in the latter cases. Therefore, LMF acted as an electron donor, and could react with PPIX that was expected to be an aggregate. Finally, it was noted that under the effect of the interaction between LMF and

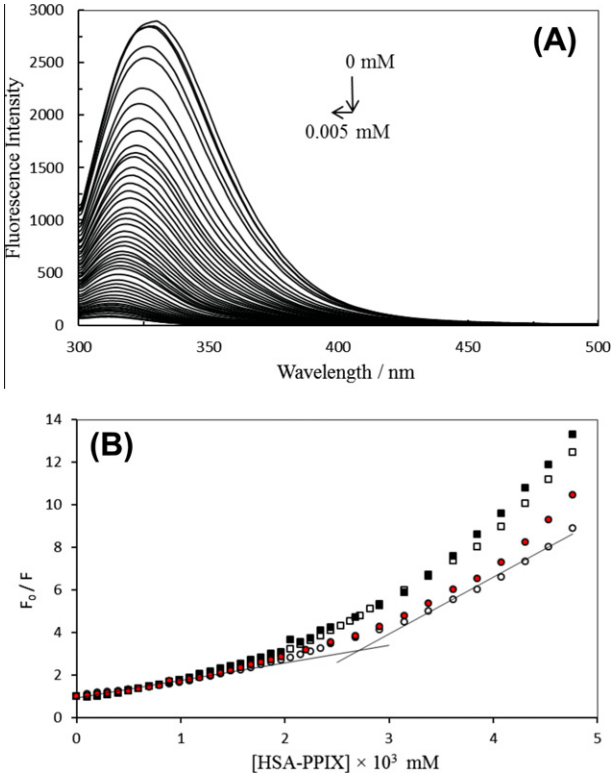

Fig. 3. (A) Fluorescence emission spectra of TF (4.5×10^{-3} mM) with various amount of HSA–PPIX following excitation at 280 nm, (B) Stern–Volmer quenching plot of free TF and the TF–LMF system with various amount of HSA–PPIX, following excitation at 280 nm. [TF] filled square, [TF–LMF (0.003 mM)] open square, [TF–LMF (0.006 mM)] filled circle and [TF–LMF (0.009 mM)] open circle.

HSA–PPIX complex, there was only gradual increase intensity at 490 nm wavelength (Fig. 2D inset), whereas in the presence of TF (Fig. 2C), we could observe an increased aggregation followed by a gradual decrease. The RLS for the aggregate clearly indicates that the size of the aggregate is large enough to scatter the light and (unlike the micellized monomer, which does not show RLS) there are multiple porphyrin molecules per aggregate. This conclusion of multiple porphyrins per aggregate is consistent with the decrease in the fluorescence quantum yield of the aggregate (Fig. 2B). When compared to the monomer because of self-quenching and excitonic interactions among porphyrins in close proximity [31]. According to this observation, we conclude that aggregation was increase in the presence of TF and protein–protein interaction than LMF (HSA–PPIX) interaction.

Fluorescence spectra

There are three intrinsic fluorophores, namely the Trp, Tyr, and Phe residues, in proteins. However, the intrinsic fluorescence of TF and HSA comes almost solely from Trp. Fluorescence quenching has been widely used to reveal the combined position of quenchers to the fluorophore. Here, the objective was to investigate protein–protein interactions (PPIs). It is known that PPIX can quench the fluorescence of Trp 214 in HSA [10], wherefore it is possible to show this phenomenon (PPIs) by quenching experiments in the absence and presence of LMF.

Fig. 3A reveals the effect of the HSA–PPIX complex as a quencher on the fluorescence of the TF at $\lambda = 280$ nm. TF emitted strong intrinsic fluorescence at 329 when it was excited at 280 nm. It was observed that the fluorescence intensity of TF decreased regularly with an increasing concentration of HSA–PPIX complex. This quenching was accompanied by a blue shift of the emission maximum wavelength of TF, which indicated that PPIs occurred and that the fluorescence residues of proteins were located at the interface of the formed complex or was brought to a more hydrophobic environment causing a change of the conformation of the protein [33,34].

There exist two fluorescence quenching processes, static and dynamic quenching. Dynamic quenching is described by the Stern–Volmer equation [31]:

$$F_0/F = 1 + K_q\tau_0[Q] \quad (2)$$

where F_0 and F are the fluorescence intensities in the absence and presence of a quencher, k_q is the bio-molecular quenching constant, τ_0 is the lifetime of the fluorophore in the absence of a quencher, and [Q] is the quencher concentration. Fig. 3B shows a Stern Volmer plot of the TF induced by HSA–PPIX complex in the absence and presence of varying concentrations of LMF (0.003, 0.006, and 0.009 mM) at $\lambda_{ex} = 280$, in order to investigate the effect of LMF on PPIs. As can be further seen in Fig. 3B, the Stern–Volmer plot presents negative divergences from linearity, following a hyperbolic-like behavior. In general, these situations result from the existence of more than one class of fluorophores, with varying K_{sv} values. In this case, the fluorescence data can be analyzed using the Lehrer equation [35].

As reported in Table 1, the K_{sv} and k_q values decrease when increasing the LMF concentration. The decrease in k_q is attributed to limitation of the quencher to access to fluorophores moieties of proteins [36]. From Table 1, it can be stated that k_q at $\lambda_{ex} = 280$ was slightly higher than when excited at 295, The comparison of fluorescence quenching of a protein excited at 280 and 295 nm renders it possible to estimate the participation of Trp and Tyr residues in the complex. Though it is believed that both Trp and Tyr residues took part in the interaction. The bio-molecular quenching constant for dynamic quenching was less than 1.0×10^{11} L/mol s and therefore all systems employed the static quenching mechanism. Data given in Fig. 3B and Table 1 indicate that, in the presence of saturating amounts of LMF, the affinity of HSA–PPIX complex for TF decreased, suggesting less protein–protein interactions.

To investigate the effect of PPIX on the binding of LMF to TF–HSA complex, the related steady-state fluorescence spectra of the

Table 1
Stern–Volmer quenching constant of the TF–(HSA–PPIX) complex with different concentrations of LMF at $\lambda_{ex} = 280$ and $\lambda_{ex} = 295$ nm.

Sample	$\lambda_{ex} = 280$		$\lambda_{ex} = 295$	
	K_{sv1}	k_{q1}	K_{sv2}	k_{q2}
TF–(HSA–PPIX)	1.22×10^6	1.22×10^{14}	7.31×10^5	7.31×10^{13}
	5.35×10^6	5.35×10^{14}	1.69×10^6	1.69×10^{14}
[TF–(HSA–PPIX)]–LMF(0.003 mM)	1.11×10^6	1.11×10^{14}	5.30×10^5	5.30×10^{13}
	4.13×10^6	4.13×10^{14}	1.13×10^6	1.13×10^{14}
[TF–(HSA–PPIX)]–LMF(0.006 mM)	1.02×10^6	1.02×10^{14}	4.4×10^5	4.4×10^{13}
	4.33×10^6	4.33×10^{14}	1.09×10^6	1.09×10^{14}
[TF–(HSA–PPIX)]–LMF(0.009 mM)	8.27×10^5	8.27×10^{12}	5×10^4	5×10^{12}
	2.66×10^6	2.66×10^{14}	5×10^5	5×10^{13}

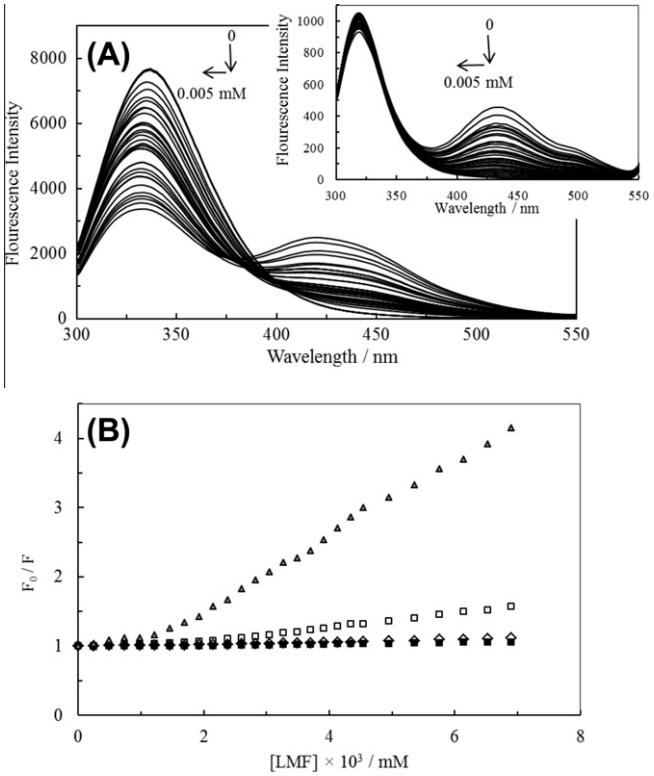

Fig. 4. (A) Fluorescence emission spectra of TF–HSA system (Inset; TF–(HSA–PPIX)) system with various amounts of [LMF] following excitation at 280 nm, and (B) Stern–Volmer quenching plot of [TF–HSA] open square, [TF–(HSA–PPIX)] filled square, free HSA filled triangle and free HSA–PPIX open triangle, with various amount of [LMF] = 0.05 mM following excitation at 280 nm, [LMF] = 0.05 mM, [TF–HSA] = [TF–(HSA–PPIX)] = [HSA] = [HSA–PPIX] = [TF] = 4.5×10^{-3} mM.

TF–HSA and TF–HSA–PPIX complex systems were obtained in Fig. 4A. According to the figure, LMF gave rise to a decrease in the fluorescence intensity. This was accompanied by a blue shift in the maximum emission peak, which was due to the fact that, in the presence of LMF, the local environment around Trp and Tyr rearranged in such a way that fluorescence residues found themselves in a more hydrophobic environment of the protein matrix [37].

The calculated K_{sv} values for TF–HSA and TF–(HSA–PPIX) complex were 4.07×10^4 and $2.3 \times 10^3\ M^{-1}$, respectively. Consequently, LMF displayed less binding than TF–(HSA–PPIX) complex to TF–HSA; in fact, the presence of PPIX resulted in a reduction of binding.

According to the fluorescence spectrum of Fig. 4A (inset), there was a new peak at about 500 nm. The emission wavelengths of 430 nm related to LMF [38] and the spectral peak observed in the fluorescence excitation spectra at about 490 nm can be attributed to the J-band of the PPIX [24,25,39]. As described in the previous section both the fluorescence and RLS spectra point to the existence of a J-aggregate.

It is known under the effect of an interaction with PPIX, LMF induced J-aggregation under the experimental conditions. Furthermore, the free PPIX plasma level may increase in patients under drug therapy as a consequence of heterotopic interaction.

To investigate the effect of TF on the affinity of LMF toward HSA and HSA–PPIX complex, Stern–Volmer plots were obtained for the HSA–LMF, (HSA–PPIX)–LMF, (TF–HSA)–LMF, and [(TF–(HSA–PPIX)]–LMF systems (Fig. 4B). It was found that the K_{sv} values for HSA and HSA–PPIX complex were 2.06×10^5 and $9.65 \times 10^3\ M^{-1}$, respectively. However, in the presence of TF, the values decreased to $4.07 \times 10^4\ M^{-1}$ for HSA and $2.36 \times 10^3\ M^{-1}$ for HSA–PPIX complex. These results clearly indicate that TF could induce structural changes in the three-dimensional conformation of albumin leading to local perturbations of the LMF binding site on HSA and HSA–PPIX complex.

Table 2
Maximum emission wavelengths and REES of HSA, TF and HSA–PPIX complex as a function of LMF and their interaction. The REES values obtained from corrected emission spectra by inner filter method.

Sample	Molar ratio/1:1	$\lambda_{em\ max}$(nm)		REES (nm)
		λ_{ex}: 295 nm	λ_{ex}: 305 nm	
HSA–LMF		341	346	5
TF–LMF		332	346	5
(HSA–TF) LMF		338	347	11
(HSA–PPIX)–LMF		330	343	13
[(HSA–PPIX)–TF] LMF		320	340	20

Red edge excitation shift (REES)

REES represents a powerful approach that can be used to directly monitor the environment and dynamics around a fluorophore in a complex biological system [40–41]. REES gives rise to slow rates of solvent relaxation around a fluorophore in an excited state, which depends on the motional restriction imposed on the solvent molecules in the immediate vicinity of the fluorophore [42]. The REES values obtained in the present study are shown in Table 2. Such dependence of the emission maximum on the excitation wavelength is characteristic of REES. According to Table 2, the REES values of HSA–LMF and TF–LMF were 5 and 6 nm, respectively (here, TF is a multi-Trp peptide, wherefore the red-edge excitation shift may be indicative of average environment experienced by the Trp). These results indicate that the Trp moieties of the HSA and TF are located in a more motionally restricted environment in the presence of LMF. In contrast, in the case of the HSA–PPIX complex conformation, the REES value was 13 nm suggesting that the average environment of the Trp residues in the HSA–PPIX complex conformation was less dynamic than for HSA.

It is known that the presence of several potential hydrogen-bonding groups within a 5 Å radius of the indole-NH group is the most probable source of the restriction of solvent dipolar reorientation in this region [43]. From the crystal structure of HSA–PPIX complex one can observe that LMF had two hydrogen bands near the Trp residue in the presence of PPIX, and this implies that the Trp was localized in a motionally restricted region. In the presence of TF in these systems and under the effect of PPI, there occurred a large REES effect, possibly due to a decrease in water content as a result of PPI and the fact that any water molecules in the immediate environment of this complex became subject to interactions with these residues. When HSA–PPIX complex was present in the complex, TF–HSA complex analogs exhibited a significant REES effect and it was thus probable that the solvent molecules in the vicinity of these naturally occurring Trp residues were involved in dipolar, electrostatic, and/or hydrogen-bonding interactions. Overall, the environment predicted for each Trp residue from the magnitude of the observed REES-values was in good agreement with previous studies of the Trp environment.

Three-dimensional fluorescence spectra

Three-dimensional fluorescence spectroscopy has become a popular technique in recent years. Fig. 5 shows 3D fluorescence spectra of TF titrated by HSA–PPIX complex in the absence and presence of LMF at three different concentrations. The fluorescence parameter including peak locations, fluorescence intensity, and

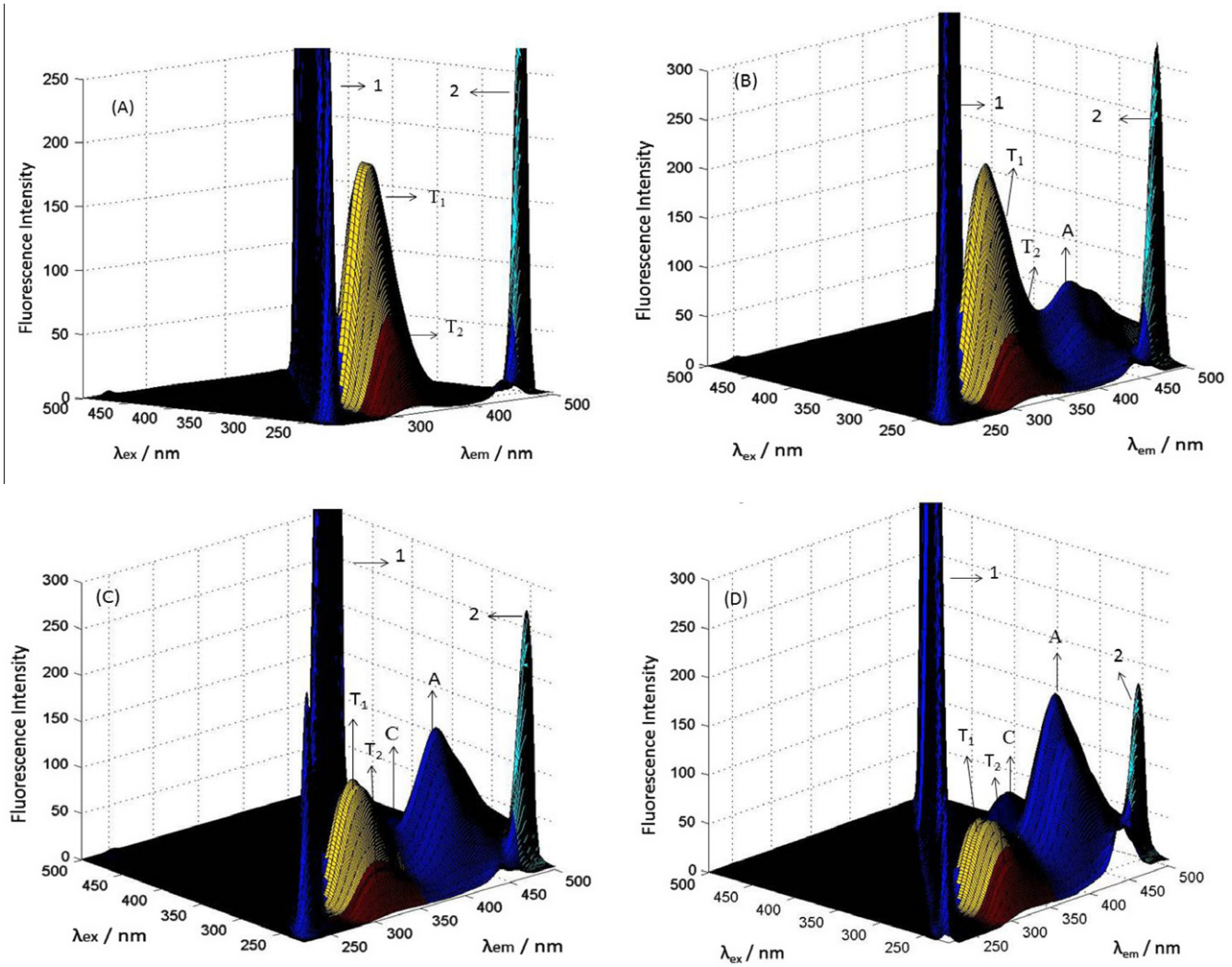

Fig. 5. Three-dimensional florescence spectra of TF–(HSA–PPIX) in the absence and presence of LMF. (A) TF–(HSA–PPIX) system, (B) [TF–(HSA–PPIX)]–(LMF 0.003 mM), (C) [TF–(HSA–PPIX)]–(LMF 0.006 mM), (D) [TF–(HSA–PPIX)]–(LMF 0.009 mM).

Table 3
Characteristics from three-dimensional fluorescence spectroscopy of the interaction of TF–(HSA–PPIX) complex in the absence and presence of LMF. [TF] = 4.5×10^{-3} mM, with or without LMF at a concentration of 0.003, 0.006 or 0.009 mM, was titrated by addition of 20 μl of [HSA–PPIX] = 1.005×10^{-5} mM at room temperature and pH = 7.4.

System	Peak T_1			Peak T_2		
	$\lambda_{ex}/\lambda_{em}$	Intensity	$\Delta\lambda$(nm)	$\lambda_{ex}/\lambda_{em}$	Intensity	$\Delta\lambda$(nm)
TF–(HSA–PPIX)	275/325	189	50	250/327	74.61	77
[TF–(HSA–PPIX)]–LMF (0.003 mM)	280/324	130.8	44	240/322	35.42	82
[TF–(HSA–PPIX)]–LMF (0.006 mM)	280/322	87.9	42	240/320	28.69	80
[TF–(HSA–PPIX)]–LMF (0.009 mM)	280/320	61.18	40	240/317	26.19	77

peak intensity ratios were extracted from the 3D fluorescence spectra, which could be employed for quantitative analysis [42,44]. There were five key fluorescence peaks that could be identified from the fluorescence spectra of the samples. The first main peak was located at the excitation/emission wavelength ($\lambda_{ex}/\lambda_{em}$) of 235–240/340–355 (peak T_2), which is mainly caused by the transition of $\pi \rightarrow \pi^*$ of the characteristic polypeptide backbone structure O═C of HSA and TF, while the second main peak was observed at the $\lambda_{ex}/\lambda_{em}$ of 280–285/320–325 (peak T_1) [45]. It is plausible that this mainly reveals the spectral characteristic of the Trp and Tyr residues, since when proteins are excited at 280 nm, the fluorescence of the Phe residue can be neglected [4]. Peaks *A* and *C* were related to a humic-like substance and natural dissolved organic matter, and are described as the LMF fluorescence [46–50].

Peak 1 was the Rayleigh scattering peak ($\lambda_{ex} = \lambda_{em}$), and peak 2 was the second-order scattering peak ($\lambda_{ex} = 2\lambda_{em}$). As is clear from Fig. 5A, HSA–PPIX complex could decrease the fluorescence intensities of peaks T_1 and T_2, suggesting that the TF with fluorescence gradually changed its conformation by interaction with HSA–PPIX complex.

The location shift of the fluorescence peak provided spectral information on the chemical structural changes of the protein samples. Upon introduction of LMF (Fig. 5A–D), the location of the T_1 and T_2 fluorescence peaks shifted toward shorter wavelengths

(blue shift), however to different extents (Table 3). A red shift is related to the increase of carbonyl, hydroxyl, alkoxyl, amino, and carboxyl groups in the structures of fluorophores, while a blue shift is ascribed to the elimination of particular functional groups such as carbonyl, hydroxyl and amine, involving a reduction in the degree of π-electron systems and a lowering of the number of aromatic rings and conjugated bonds in a chain structure [44]. The observation of blue shifts and drops in intensity for peaks T_1 and T_2 in the presence of LMF agreed well with the results of both fluorescence and RLS. Moreover, with the increase in the concentration of LMF and the decrease in peaks T_1, T_2, an increase in peaks A and C was observed with the blue shift. There was thus a specific interaction between TF and HSA–PPIX complex, and LMF could influence their interaction by affecting the protein conformation.

Circular dichroism (CD) spectroscopy

Circular dichroism (CD) spectroscopy is a sensitive technique when it comes to monitoring conformational changes in a protein upon interaction with a ligand [33]. Far UV CD spectra (190–250 nm) of the proteins were recorded at room temperature. In this study, the titration of HSA and HSA–PPIX complex by TF was used in the absence and presence of LMF at three different concentrations (Fig. 6). The CD spectra of the protein exhibited two negative bands at 208 and 222 nm which were the characteristic of a α-helix in the advanced structure of the protein [16]. The reasonable explanation was that the negative peaks near 208 and 222 nm both contributed to the $n \rightarrow \pi^*$ transfer for the bond of the α-helix [4]. If the α-helixes changed, the spectra would change accordingly. As a can be seen from Fig. 6, the ellipticity of the complexes of [TF–(HSA–PPIX)] complex (inset) and HSA at 222 and 208 nm increased, which suggests the gain of α-helical content in both proteins after complex formation.

In the presence of 0.001, 0.002, 0.003 mM LMF, the secondary structural contents were measured and are shown in Table 4. As can be seen, there was a significant loss of helix content in the TF–HSA or [TF–(HSA–PPIX)] complex systems with increasing LMF concentration. This was probably due to a disruption of inter-domain and intra-domain structure. As known, the secondary structure contents are closely related to the biological activity of the protein, and there was thus a decrease in α-helical content

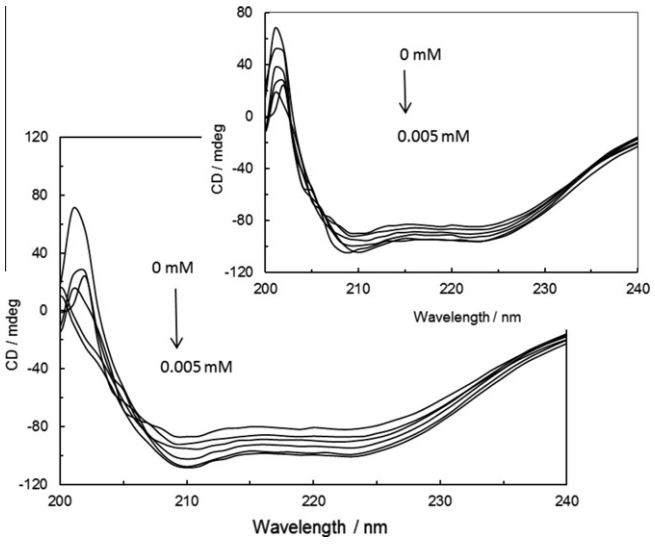

Fig. 6. CD spectra of the; TF–HSA system and (inset); TF–(HSA–PPIX) system in the presence and absence of three concentration of LMF. [TF] = 1.5 μM, [HSA] and [HSA–PPIX] = 33.5 × 10^{-3} mM, [LMF] = 0.001, 0.002 and 0.003 mM.

Table 4
Fraction of the secondary structure of the TF–HSA and TF–(HSA–PPIX) complex systems in the absence and presence of LMF at different concentrations (pH 7.4).

System	f_α	f_β	f_T	f_U
TF	37.1	28.3	15.3	19.1
TF–HSA	40.19	27.05	14.94	17.82
[TF–HSA]–LMF (0.003 mM)	37.21	25.73	14.02	23.04
[TF–HSA]–LMF (0.006 mM)	35.03	24.22	14.08	26.67
[TF–HSA]–LMF (0.009 mM)	30.35	21.17	13.72	34.76
TF–(HSA–PPIX)	38.85	27.97	15.14	18.04
[TF–(HSA–PPIX)]–LMF (0.003 mM)	35.17	26.42	14.71	23.70
[TF–(HSA–PPIX)]–LMF (0.006 mM)	32.25	24.83	14.27	28.65
[TF–(HSA–PPIX)]–LMF (0.009 mM)	31.11	22.73	13.52	32.64

f_α, f_β, f_T, and f_U are the fraction of α-helix, β-sheet, turn and unordered coil respectively.

from 40.19 to 35.03 for the TF–HSA solutions and from 38.85 to 31.11 for the TF–(HSA–PPIX) complex solutions in the presence of LMF. This meant a loss of the biological activity of the proteins in blood plasma. The secondary structural changes induced by interaction of HSA with PPIX could be monitored by comparing the TF–HSA and TF–(HSA–PPIX) complex systems. It was observed that, in the presence of PPIX, the fraction of α-helical and β-sheet contents decreased whereas the fraction of turn and unordered coil increased. These results suggest the occurrence of conformational changes at the secondary structural level in the reaction between PPIX and HSA.

Binding distance between the drug and protein

Fluorescence energy transfer is categorized as radiation energy transfer and non-radiation energy transfer. the energy transfer of the proteins and LMF should be of non-radiation type. Non-radiation energy transfer consists of inter-molecular and intra-molecular energy transfer, and the fluorescence quenching of HSA, HSA–PPIX complex and TF should belong to the type inter-molecular non-radiation energy transfer [46] for the reasons detailed below.

According to Förster's non-radiative energy transfer theory (FRET), if the emitted fluorescence from a donor can be absorbed by an acceptor, energy may transfer from the donor to the acceptor [51]. FRET is an interaction that depends strongly on the distance between the donor and the acceptor. But it is not the only factor influencing the efficiency of the process. The efficiency of FRET is based on the following factors: (i) the extent of overlap between the donor emission and the acceptor absorption, (ii) the orientation of the transition dipole of the donor and acceptor, and (iii) the distance between the donor and acceptor [51–52]. Fig. 7 A and B shows the values of the distance between the donor and acceptor that were found to be the following: r = 2.02 nm for HSA, 1.79 nm for TF, 1.82 nm for HSA–PPIX complex, 2.71 nm for TF–HSA and 2.13 nm for TF–(HSA–PPIX) complex in the presence of LMF. It can thus be seen that the donor-to-acceptor distance (r) was much smaller than 7 nm, which indicates that the energy transfer from fluor residues to LMF occurred with a high probability. Consequently, static quenching and non-radiation energy transfer were the main reasons leading to the fluorescence quenching.

Zeta potential

The surface properties of proteins, and especially their surface electrical properties, have an important influence on their ionic interactions with other biomacromolecules. The surface charge of proteins arises primarily from ionization of surface groups [53]. Most proteins have hydrophobic nonpolar residues, such as alkyl

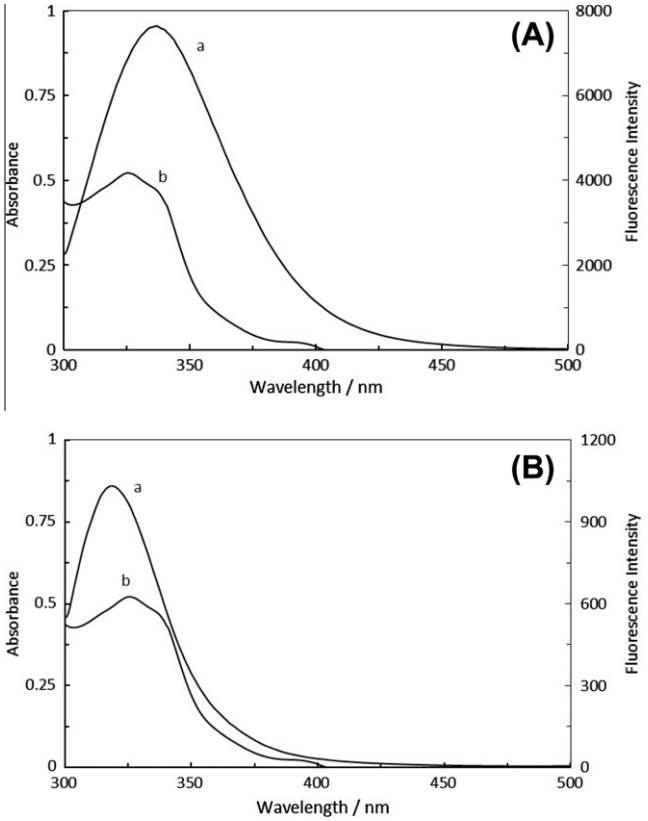

Fig. 7. Spectral overlap of the fluorescence spectra (curves a) of (A) [TF–HSA] and (B) [TF–(HSA–PPIX)] system, with absorption spectra (curves b) of LMF. [HSA] = [HSA–PPIX] = [TF] = [LMF] = 4.5×10^{-3} mM.

and aromatic groups, ionic groups such as $-NH^{+3}$ and COO^{-}, as well as hydrophilic polar groups such as –OH and $-NH_2$. The charge on a protein can be estimated from the sum of the charge on the individual amino acid residues. The net charge is dominated by a positive contribution from Lys and His and increasingly negative contributions from aspartic and glutamic acid. Other amino acids carry charge but are not present on an adequate mass basis to influence the total charge [54–55].

The charge properties of proteins and the zeta potential of the interaction between TF–HSA and TF–(HSA–PPIX) complex in the absence and presence of LMF are shown in Fig. 8A and B, respectively. As the protein charge is usually low, and electrophoresis is carried out at normal ionic strength [54]. Fig. 8 exhibits increasing positive charges on the protein surface at the interaction with HSA and HSA–PPIX complex. TF has a net negative global charge and therefore the electrostatic interaction between TF and HSA is triggered by negatively charged TF and positive charges of the cationic groups in HSA. The change of the zeta potential was associated with chain entanglements; therefore, the system became incipiently instable [53]. Finally at higher HSA concentrations, the zeta potential became more negative. This negative value of the zeta potential suggests that hydrophobic interactions were predominant. The change in the zeta-potential zone started close to the critical induced aggregation concentration (C_{CIAC}) of the HSA or HSA–PPIX complex in the case of these proteins, which indicates that the protein surface was saturated and that aggregation of the HSA or HSA–PPIX complex was reached [54].

The inclusion of LMF in the system contributed to the net surface charge since the LMF used in this work exhibited a net neutral charge. However, the presence of LMF could cause a decrease in the positive charge of TF–HSA by a conformational change in the protein.

We hypothesized that the LMF complex was involved in a certain neutralization of the net protein charge and that a protein conformational change allowed the electrostatic attraction to decrease. This led to the C_{CIAC} point being achieved at a lower concentration of HSA. However, when increasing the LMF concentration there was a restructuring in the protein causing the complex to become more negative. It also led to electrostatic repulsion between the carboxylate groups competing with the hydrophobic interactions between the two proteins. This gave rise to an increase in the hydrophobic interaction of the complex, leading to precipitation at low HSA concentration. This hypothesis was in agreement with important losses of tertiary and secondary structure as observed in the results of the fluorescence measurements, RLS and CD spectroscopy at increasing LMF concentrations. As shown in Fig. 8B, in the presence of HSA–PPIX complex, the system reached the C_{CIAC} sooner and the net negative charge increased. Moreover, there occurred an increase of hydrophobic interactions with the rise in LMF concentration by loss of polar contacts.

The polydispersity index (PDI) was also determined by the zeta potential method [56–57]. The polydispersity of TF was measured during titration with HSA or HSA–PPIX complex in the absence and presence of LMF at different concentrations. The results are shown in Fig. 8(C, D). The PDI is the ratio of the mass average degree of the molecular weight to the number average degree of the molecular weight. The size distribution was given by the polydispersity index (a value between 0 and 1). A PDI of 1 indicates large variations in particle size; a PDI of 0 indicates no variation in particle size (as an ideal monodispersed formulation) [58–61]. A significant increase in PDI was observed upon increasing the LMF concentration. The PDI value for the TF–(HSA–PPIX) complex system was greater than for TF–HSA and indicated that the TF–(HSA–PPIX) complex population prepared with a 1/1 charge ratio was more heterogeneous than the TF–HSA system in the presence of LMF.

The homogeneity of the (TF–HSA) LMF solution was supported by lower PDI values. On the other hand, the higher PDI value of (TF–HSA–PPIX) LMF suggests the existence of large aggregates of PPIX when LMF is present.

Molecular modeling

To further realize the interaction of LMF with HSA, TF, and HSA–PPIX complex, interaction models were produced using molecular modeling techniques. Autodock 4 was used to determine the best docking result. It was found that the inhibiting constant for HSA was lower than for the other proteins as well as for TF and HSA–PPIX complex. We know that LMF binds to site IB of HSA [9]. Here, we observed binding-site switching in the presence of PPIX, and LMF thus bound to site IIA of HSA. The best docking results for the (HSA–PPIX)–LMF are shown in Figs. 9 and 10 and the distance between LMF and Trp 214 was determined from this model. It is important to note that in the presence of PPIX, the distance between LMF and Trp 214 was 2.52 Å, which coincided with the very efficient fluorescence quenching of HSA emission in the presence of LMF and PPIX. Ligand binding to one domain induced distance conformational changes in other domains. Therefore, the distance between the centers of PPIX to Trp 214 was determined in the absence and presence of LMF. It was found to be 25.16 Å without LMF and decreased to 24.77 Å in the presence of LMF.

To get a better understanding of protein–protein interactions in the presence of LMF, the HEX software was used to deduce the best docking result of interaction between TF–HSA or TF–(HSA–PPIX) complex in the presence of LMF. The results pointed at TF–HSA having a lower binding energy while that of TF–(HSA–PPIX) complex was higher in the presence of LMF. It was also found that the presence of PPIX and LMF changed the angle of interaction between the two proteins, which can explain the covering of the site

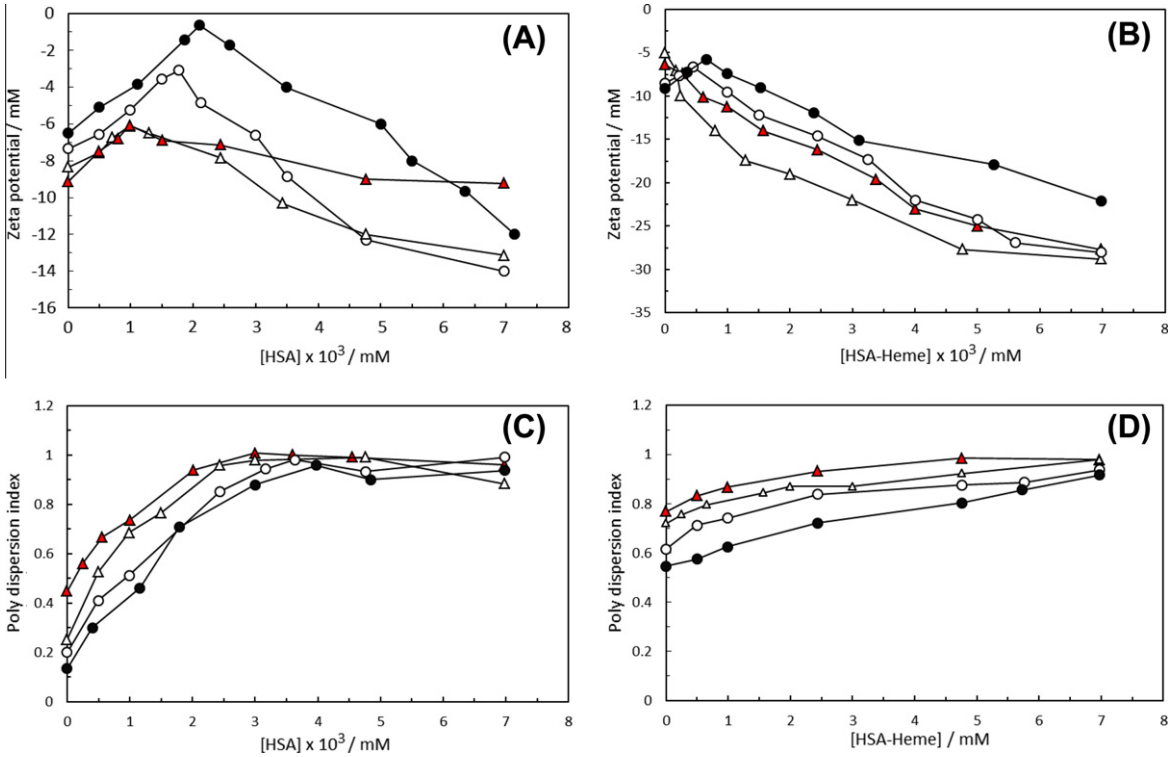

Fig. 8. Effect of (A); HSA and (B); HSA–PPIX on the zeta potential of the TF–LMF system in pH 7.4,(C); Effect of the HSA and (D); HSA–PPIX in the poly-dispersion index of the TF–LMF system, free TF filled circle, [TF–LMF(0.003 mM)] open circle, [TF–LMF(0.006 mM)] filled triangle and [TF–LMF(0.009 mM)] open triangle.

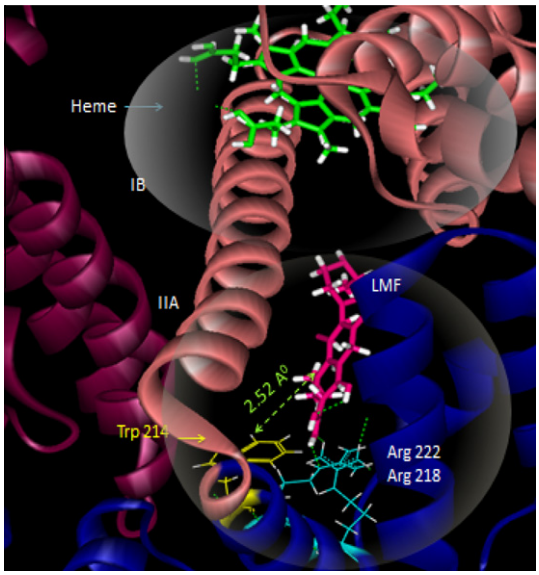

Fig. 9. Molecular modeling of the interaction of LMF with HSA–PPIX represented in as a solid ribbon, colored by the secondary structure, LMF represented as a stick. LMF has been docked into the sub-domain IIA for HSA–PPIX. The distance between the candidates' binding sites of LMF to Trp is also illustrated. The hydrogen bonds between LMF and HSA–PPIX are represented was green dashed lines. (For interpretation of the references to color in this figure legend, the reader is referred to the web version of this article.)

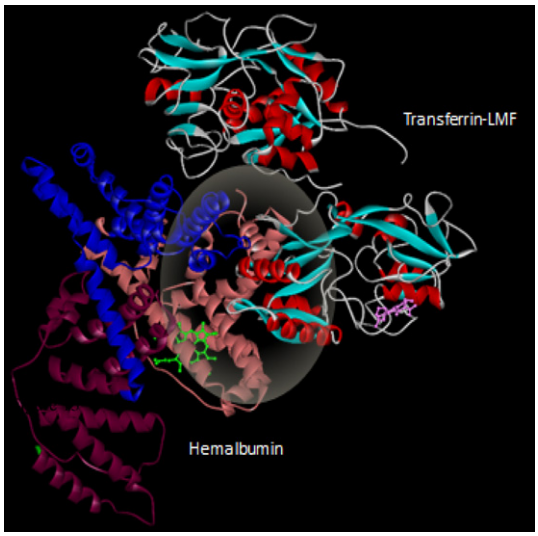

Fig. 10. Molecular modeling of the interaction of [TF–LMF] with HSA–PPIX, TF and HSA–PPIX are represented as solid ribbons, colored by the secondary structure, and the three domains are illustrated by different colors in HSA–PPIX. Domain I (residues 1–195) is pink, domain II (residues 190–383) is blue and domain III (residues 384–585) is purple. (For interpretation of the references to color in this figure legend, the reader is referred to the web version of this article.)

of interaction of the ligands with the protein. As was seen, maximum coverage occurred when PPIX was present while occupying site IB. Such a behavior of PPIX might explain the lower acceptance of LMF in this protein.

Conclusions

Here it was shown that the PPIs (HSA–TF), and [(HSA–PPIX)–TF)] interactions decreased with the increase in LMF concentration. Aggregation of PPIX was also observed by resonance light scattering analysis at the presence of protein–protein interactions and

drug–protein interactions. We concluded that aggregation of PPIX was increased in the presence of protein–protein interaction. Fluorescence spectroscopy shown, in the presence of saturating amounts of LMF, the affinity of HSA–PPIX complex for TF decreased. Also the binding affinity of LMF to HSA–PPIX complex was lower than to HSA and became reduced by interaction with TF. These results clearly indicate that TF could induce structural changes in the three-dimensional conformation of albumin.

Furthermore, we demonstrated that HSA–PPIX complex Trp presented an increased REES result during interaction with LMF as compared to HSA and the extent of REES increased at the effect of TF. The results of the zeta potential measurements rendered it possible to verify the existence of the complexion process in relation to the reversal in the sign of protein complexes as the drug binding proceeded. This change was the first evidence of the existence of electrostatic interactions between the HSA–PPIX complex and the mixture of TF–LMF, as they differed in their net electrical charge. As a result, the hydrophobic interaction was predominant. This change in zeta potential zone started close to the C_{CIAC} of HSA–PPIX complex in the case of TF. Finally, the change of the protein conformation upon binding was monitored by fluorescence CD and molecular modeling as a function of added drug and indicated that a significant loss of helix content in TF–HSA or TF–(HSA–PPIX) systems with increasing LMF concentration. This investigation highlights the effect of other serum proteins on evaluation of the binding parameters of different ligands to other proteins in serum.

Acknowledgements

The financial support of the Research Council of the Mashhad Branch, Islamic Azad University is gratefully acknowledged. The authors thank Dr. Ljungberg for the English editing.

References

[1] Y.L. Zhou, J.M. Liao, F. Du, Y. Liang, Thermodynamics of the interaction of xanthine oxidase with superoxide dismutase studied by isothermal titration calorimetry and fluorescence spectroscopy, Thermochim. Acta 426 (2005) 173–178.
[2] L.T. Lemiesz, Paclitaxel–HSA interaction. Binding sites on HSA molecule, Bioorg. Med. Chem. 12 (2004) 3269–3275.
[3] S.M. Darwish, S.E. Abu sharhk, M.M. Abu Teir, S.A. Makharza, M.M. Abu-hadid, Spectroscopic investigations of pentobarbital with human serum albumin, J. Mol. Struct. 963 (2010) 122–129.
[4] Y.Z. Zhang, B. Zhou, X.P. Zhang, P. Huang, C.H. Li, Y. Liu, Interaction of malachite green with bovine serum albumin: determination of the binding mechanism and binding site by spectroscopic methods, J. Hazard. Mater. 163 (2009) 1345–1352.
[5] J. Wang, Z. Liu, J. Liu, S. Liu, W. Shen, Study on the interaction between fluoroquinolones and erythrosine by absorption, fluorescence and resonance Rayleigh scattering spectra and their application, Spectrochim. Acta Part A 69 (2008) 963–965.
[6] J.L. Yuan, Z. Iv, Z.G. Liu, Z. Hu, G.L. Zou, Study on interaction between apigenin and human serum albumin by spectroscopy and molecular modeling, J. Photochem. Photobiol. A 191 (2007) 104–113.
[7] H. Vahedian-Movahed, M.R. Saberi, J. Chamani, Comparison of binding interactions of lomefloxacin to serum albumin and serum transferrin by resonance light scattering and fluorescence quenching methods, J. Biomol. Struct. Dyn. 28 (2011) 483–502.
[8] M. Zhang, D.R. Gumerov, I.A. Kaltashov, Indirect detection of protein–metal binding:interraction of serum transferrin with In+3and Bi+3, J. Am. Soc. Mass Spectrom. 15 (2004) 1658–1664.
[9] J. Chamani, H. Vahedian-Movahed, M.R. Saberi, Lomefloxacin promotes the interaction between human serum albumin and transferrin: a mechanistic insight into the emergence of antibiotic's side effects, J. Pharm. Biomed. Anal. 55 (2011) 114–124.
[10] A.K. Shaw, S.K. Pal, Resonance energy transfer and ligand binding studies on pH-induced folded states of human serum albumin, J. Photochem. Photobiol. B 90 (2008) 187–197.
[11] S.S. Kalanur, J. Seetharamappa, A. Kalalbandi, charechterization of interaction and effect of carbamazepine on the structure of human serum albumin, J. Pharm. Biomed. Anal. 53 (2010) 660–666.
[12] M. Wardell, Z. Wang, J.X. Ho, J. Robert, The atomic structure of human methemalbumin at 1.9 A, Biochem. Biophys. Res. Commun. 291 (2002) 813–819.
[13] P. Ascenzi, A. Bocedi, S. Notari, E. Menegatti, M. Fasano, Heme impairs allosterically drug binding to human serum albumin Sudlow's site I, Biochem. Biophys. Res. Commun. 334 (2005) 481–486.
[14] S.V. Bhosalea, M.B. Kalyankarb, S.V. Bhosaleb, S.G. Patila, C.H. Lalandera. S.J. Langforda, S.V. Nalage, Supramolecular self-assembly of protoporphyrin IX amphiphiles in to worm-like and particular aggregares, Supramol. Chem. 23 (2011) 263–268.
[15] X.M. He, D.C. Carter, Atomic structure and chemistry of human serum albumin, Nature 358 (1992) 209–215.
[16] M. Cheema, P. Taboada, S. Barbosa, J. Juarez, M.G. Pichel, M. Siddiq, V. Mosquera, Human serum albumin unfolding pathway upon drug binding: athermodynamic and spectroscopic description, J. Chem. Thermodyn. 41 (2009) 439–447.
[17] L. Wang, L. Wang, H. Chen, L. Li, L. Dong, T. Xia, F. Dong, Z. Xu, Direct quantification of γ-globulin in human blood serum by resonance light scattering techniques without separation of human serum albumin, Anal. Chim. Acta 493 (2003) 179–184.
[18] Z. Chen, X. Liao, L. Zhu, J. Liu, Y. Han, Micro-determination of nucleic acids with a simple probe manganese chloride based on the fine enhanced resonance light scattering, Spectrochim. Acta Part A 68 (2007) 263–268.
[19] Z. Wang, N.R. Kumar, D.K. Srivasva, A novel spectroscopic titration method for determining the dissociation constant and stoichiometry of protein–ligand complex, Anal. Biochem. 206 (1992) 376–381.
[20] C.Z. Huang, Y.F. Li, Resonance light scattering technique used for biochemical and pharmaceutical analysis, Anal. Chim. Acta 500 (2003) 105–117.
[21] J.R. Lakowicz, Principle of Fluorescence Spectroscopy, Springer Science+Business Media, New York, 2006. pp. 52, 277, 530.
[22] Y. Chen, D. Gao, Y. Tian, P. Ai, H. Zhang, A. Yu, Resonance light scattering technique for the determination of proteins with polymethacrylic acid(PMAA), Spectrochim. Acta Part A 67 (2007) 1126–1130.
[23] M.Y. Choi, J.A. Pollard, M.A. Webb, J.L. Mchale, Counterion-dependent excitionic spectra of tetra (p-carboxyphenyl) porphyrin aggregates in acidic aqueous solution, J. Am. Chem. Soc. 125 (2003) 811.
[24] L.M. Scolaro, M. Castriciano, A. Romeo, S. Patane, E. Cefali, M. Allegrini, Aggregation behaviour of protoporphyrin IX in aqueous solutions: clear evidence of vesicle formation, J. Phys. Chem. B 106 (2002) 2453–2459.
[25] H.L. Ma, W. Jin, Studies on the effects of metal ions and counter anions on the aggregate behaviors of meso-tetrakis(p-sulfonatophenyl)porphyrin by absorption and fluorescence spectroscopy, Spectrochim. Acta Part A 71 (2008) 153–160.
[26] G.D. Luca, A. Romeo, L.M. Scolaro, Counteranion dependent protonation and aggregation of tetrakis (4-sulfonatophenyl) porphyrin in organic solvents, J. Phys. Chem. B 110 (2006) 7309–7315.
[27] Y. Zang, M. Xian, M.Y. Lu, R.H. Yang, F. Liu, K. Anli, Anion chelation-induced porphyrin protonation and its application for chloride anion sensing, J. Phys. Chem. A 109 (2005) 7442–7448.
[28] G.D. Luca, A. Romeo, L.M. Scolaro, Role of counteranions in acid-induced aggregation of isomeric tetrapyridylporphyrins in organic solvent, J. Phys. Chem. B 109 (2005) 7149–7158.
[29] G. Deluca, A. Romeo, L.M. Scolaro, Counteranion dependent protonation and aggregation of Tetrakis (4-sulfonatophenyl) prophyrin in organic solvent, J. Phys. Chem. B 110 (2006) 7309–7315.
[30] J. Parkash, J.H. Robblee, J. Agnew, E. Gibbs, P. Collings, R.F. Pasternack, J.C. de Paula, Depolarized resonance light scattering by porphyrin and chlorophyll a aggregates, Biophys. J . 74 (1998) 2089–2099.
[31] N.C. Maiti, S. Mazumdar, N. Periasamy, J-and H-aggregates of porphyrin-surfactant complexes: time-resolved fluorescence and other spectroscopic studies, J. Phys. Chem. B 102 (1998) 1528–1538.
[32] T. Hirano, S. Yasuda, Y. Osaka, M. Kobayashi, S. Itagaki, K. Iseki, Mechanism of the inhibitory effect of zwitterionic drugs (levofloxacin and grepafloxacin) on carnitine transporter(OCTN2) in Caco-2 cells, Biochim. Biophys. Acta 1758 (2006) 1743–1750.
[33] L. Trynda-Lemiesz, Paclitaxel–HSA interaction. Binding sites on HSA molecule, Bioorg. Med. Chem. 12 (2004) 3269–3275.
[34] J. Chamani, N. Tafrishi, M. Momen-Heravi, Characterization of the interaction between human lactoferrin and lomefloxacin at physiological condition: multi-spectroscopic and modeling description, J. Lumin. 130 (2010) 1160–1168.
[35] S.S. Lehrer, Solute perturbation of protein fluorescence. The quenching of the tryptophyl fluorescence of model compounds and lysozyme by iodide ion, Biochemistry 10 (1971) 3254–3263.
[36] O. Rinco, J. Brenton, A. Douglas, A. Maxwell, M. Henderson, The effect of porphyrin structure on binding to human serum albumin by fluorescence spectroscopy, Photochem. Photobiol. A 208 (2009) 91–96.
[37] S. Sarzehi, J. Chamani, Investigation on the interaction between tamoxifen and human holo-transferrin: determination of the binding mechanism by fluorescence quenching, resonance light scattering and circular dichroism methods, Int. J. Biol. Macromol. 47 (2010) 558–569.
[38] Y. Ni, S. Su, S. Kokot, Spectrometric studies on the interaction of fluoroquinolones and bovine serum albumin, Spectrochim. Acta Part A 75 (2010) 547–552.
[39] J. Valanciunaite, S. Bagdonas, G. Streckyte, R. Rotomskis, Spectroscopic study of TPPS4 nanostructures in the presence of bovine serum albumin, Photochem. Photobiol. Sci. 5 (2006) 381–388.
[40] Chattopadhyay, Exploring membrane organization and dynamics by the wavelength-selective fluorescence approach, Chem. Phys. Lipids A 122 (2003) 3–17.

[41] H. Raghuraman, D.A. Kelkar, A. Chattopadhyay, Novel insights in to membrane protein stracture and dynamics utilizing the red edge excitation shift, in: C.D. Gedds, J.R. Lakowicz (Eds.), Reviews in Fluorescence, vol. 2, Springer, New York, 2005, pp. 199–222.
[42] H.M. Zhang, Y.Q. Wang, M. Jiang, A fluorimetric study of the interaction of CI Solvent Red 24 with haemoglobin, Dyes. Pigm. 82 (2009) 156–163.
[43] M.C. Tory, A.R. Merrill, Determination of membrane protein topology by red-edge excitation shift analysis: application to the membrane-bound colicin E1 channel peptide, Biochim. Biophys. Acta 1564 (2002) 435–448.
[44] T. Liu, Z. Chen, W. Yu, S. You, Characterization of organic membrane foulants in a submerged membrane bioreactor with pre-ozonation using three-dimensional excitation-emission matrix fluorescence spectroscopy, Water Res. 45 (2011) 2111–2121.
[45] Z. Wang, Z. Wu, S. Tang, Characterization of dissolved organic matter in a submerged membrane bioreactor by using three-dimensional excitation and emission matrix fluorescence spectroscopy, Water Res. 43 (2009) 1533–1540.
[46] G. Sheng, H. Yu, Characterization of extracellular polymeric substances of aerobic and anaerobic sludge using three-dimensional excitation and emission matrix fluorescence spectroscopy, Water Res. 40 (2006) 1233–1239.
[47] D. Patra, A.K. Mishra, Excitation-emission matrix spectral subtraction fluorescence to check adulteration of petrol kerosene, Appl. Spectrosc. 55 (2001) 338–342.
[48] M.L. Nahorniak, K.S. Booksh, Excitation–emission matrix fluorescence spectroscopy in conjunction with multiway analysis for PAH detection in complex matrices, Analyst 131 (2006) 1306–1315.
[49] R.D. Holbrook, P.C. Derose, S.D. Leigh, A.L. Rukhin, N.A. Heckert, Excitation–emission matrix fluorescence spectroscopy for natural organic matter characterization: a quantitative evaluation of calibration and spectral correction, Appl. Spectrosc. 60 (2006) 791–799.
[50] H.C. Goicoechea, K. Calimag-Williams, A.D. Campiglia, Multi-way partial least-squares and residual bi-linearization for the direct determination of monohydroxy-polycyclic hydrocarbons on octadecyl membranes via room-temperature fluorescence excitation emission matrices, Anal. Chim. Acta 717 (2012) 100–109.
[51] A. Mallick, P. Purkayastha, N. Chattopadhyay, Photoprocesses of excited molecules in confined liquid environments: an overview, J. Photochem. Photobiol. C 8 (2007) 109–127.
[52] B. Liu, F. Zhao, C. Xue, J. Wang, Y. Lu, Studies on the antagonistic action between chloramphenicol and quinolones with presence of bovine serum albumin by fluorescence spectroscopy, J. Lumin. 130 (2010) 859–864.
[53] Y. Zhao, F. Li, T. Carvajal, M.T. Harris, Interactions between bovine serum albumin and alginate: an evaluation of alginate as protein carrier, J. Colloid Interface Sci. 332 (2009) 345–353.
[54] G. Prieto, J. Sabin, J.M. Ruso, A. Perez, F. Sarmiento, Colloids Surf. A 249 (2004) 51–55.
[55] A. Malhotra, J. Coupland, The effect of surfactants on the solubility, zeta potential, and viscosity of soy protein isolates, Food Hydrocolloids 18 (2004) 101–108.
[56] A. Oliveira, M. Ferraz, F. Monteiro, S. Simoes, Cationic liposome–DNA complexes as gene delivery vectors: development and behaviour towards bone-like cells, Acta Biomater. 5 (2009) 2142–2151.
[57] B. Subramanian, F. Kuo, E. Ada, T. Kotyla, T. Wilson, S. Yoganathan, R. Nicolosi, Enhancement of anti-inflammatory property of aspirin in mice by a nano-emulsion preparation, Int. Immunopharmacol. 8 (2008) 1533–1539.
[58] L. Peng, C. Liu, C. Kwan, K. Huang, Optimization of water-in-oil nanoemulsions by mixed surfactants, Colloids. Surf. A 370 (2010) 136–142.
[59] T.W. Chung, S.S. Wang, W.J. Tsai, Accelerating thrombolysis with chitosan-coated plasminogen activators encapsulated in poly-(lactide-co-glycolide) (PLGA) nanoparticles, Biomaterials 29 (2008) 228–237.
[60] G. Coue, J.F.J. Engbersen, Functionalized linear poly (amidoamine)s are efficient vectors for intracellular protein delivery, J. Controlled Release 152 (2011) 90–98.
[61] R.J. Hunter, Zeta potential in colloid Science, Academic Press, New York, NY, 1981.